Journal of Structural Engineering / Volume 142 Issue 6 - June 2016

Application of a New System of Self-Tensioning to the Design of Large-Span Wood Floor Framings

D. Otero-Chans[1], J. Estévez-Cimadevila[1], E. Martín-Gutiérrez[1], J. Pérez-Valcárcel[1]

(1) University of A Coruña, Department of Architectural, Civil and Aeronautical Building Structures, Campus A Zapateira, 15071, A Coruña, Spain.

Corresponding author: marilo@udc.es (Dolores Otero-Chans)

ORCID:https://orcid.org/0000-0003-1738-252X (Dolores Otero-Chans)
https://orcid.org/0000-0002-8460-2097 (Javier Estévez-Cimadevila)
https://orcid.org/0000-0001-7464-4288 (Emilio Martín-Gutiérrez)
https://orcid.org/0000-0002-6440-5432 (Juan Pérez-Valcárcel)

ABSTRACT: This study describes a self-tensioning system in which the gravitational loads acting on a horizontal structural element are automatically converted to a posttensioning force on that component. The self-tensioning effect has a variable intensity, constantly adjusted depending on the applied service loads. The self-tensioning is eccentrically applied over the cross section, and it generates a negative moment that compensates the deformations due to the gravitational loads. The system can be utilized in beams, slabs, and structural framings of different materials and can be implemented using different mechanical and hydraulic solutions. The study describes the operation of a mechanical solution for the self-tensioning system and analyzes its behavior in large-span timber floor framings. When combined with conventional pretensioning, the self-tensioning system notably improves the strength and deformation behavior and permits a design of timber floor framings with a total height of 0.03 times the span length, achieving relative deflections below 1/1,000 of the span for the service loads of the structure.

KEYWORDS: Posttensioning; Self-tensioning; Prestressing; Pretensioning; Tensioning systems; Long span; Timber flooring; Wooden structures.

1. Introduction

Pre-tensioning and post-tensioning forces are well known in structural elements. They are widely used in many systems and with different materials, especially concrete, as they can modify the bending stresses by reducing or canceling the tensile stresses. This property of tensioning is also useful in wooden structures. Although wood has a very high tensile strength when it is defect-free, its tensile strength in real structures is less than its compressive strength due to the presence of defects intrinsic to this material. However, wood exhibits ductile failure in compression and brittle failure in tension. As a result, the introduction of a compressive force via a tensioning system reduces the probability of brittle failures in the material, which are always undesirable in real structures.

When tensioning forces are eccentrically applied to the cross-section of a structural element, they also introduce a bending effect opposite to the gravitational loads. This effect helps to limit the final deformations, improving the behavior of structures at their serviceability limit (Palermo et al. 2010). This feature has been widely used in steel and wooden structures, especially in those with long spans inasmuch as their bigger deformations are what will most condition the design. In the case of wooden structures, these solutions have recently lead to the development of a special field of study because of the wood's low rigidity in comparison with other structural materials.

The simplest system for limiting deformation involves the use of unbonded tendons placed eccentrically on the cross-section. The maximum efficiency is reached by placing tendons externally to the cross-section, as in under-deck cable-stayed beams (Gesualdo and Lima 2012), although these designs are limited by the direct exposure of the metal tendons to fire or by the need of substantial beam heights.

Introducing the tensioning components within the cross-section, even though placed as far as possible from its barycenter, enables to use the wooden cross-section as a protective component in the case of fire. Simultaneously, the steel is not visually perceived anymore, so it seems that the structural element is entirely made of a timber piece with a height that appears smaller than it should be. These tendons can be pre-tensioned, as in the panels of the roof of the Richmond Olympic Oval in Vancouver, Canada (Long 2010), or post-tensioned, as in the solution proposed by Massey University College of Creative Arts, Wellington, New Zealand (Van Beerchoten et al. 2012).

Post-tensioning systems allows the connection of pillars and beams, resulting in an increased rigidity of the joint, thus giving the possibility of transmitting moments. This improves the behavior in comparison to beam-pillar joints made with traditional mechanical components. Several authors (Morris et al. 2012; Buchanan et al. 2011; Wanninger and Frangi 2014) have studied the use of post-tensioning systems that employ unbonded tendons to increase the rigidity of these beam-pillar joints in complete wooden frameworks. Another advantage of these systems is the improved seismic behavior of multi-story buildings entirely built with wooden structural components (Iqbal et al. 2014; Smith et al. 2014).

Another option that has traditionally been used to improve the bending behavior of wooden elements is reinforcement with bars or bonded tendons, which may be pre-tensioned. Based on the progress in adhesive technologies and their derivatives, many studies have proposed the use of Fiber Reinforced Polymer (FRP) or other fibers that are glued to the wood in the form of bands, sheets, or bars (Borri et al.

2013; De la Rosa et al. 2013; D'Ambrisi et al. 2014). Initially, these proposals were related to the development of reinforcements for existing structures. These reinforcements resulted in improvements of the strength and rigidity of these elements, although the improvements were heavily dependent on how the reinforcements were executed. In addition, it has been observed that the rigidity also increases when incrementing the span of the components (Alhayek and Svecova 2012). Reinforcement can also be performed with bonded-in steel, but several authors have noted the problem of possible failure due to delamination caused by the difference in the rigidites of the materials that are to be joined (Brunner 2004; Kliger et al. 2008).

These solutions have been extrapolated to the design of new structural elements in which the reinforcing component is pre-tensioned before bonding it to the beam. Furthermore, this approach adds a small precamber generated by the pre-tensioning to the advantages of the reinforcement (Triantafillou and Deskovic 1992; Dolan et al. 1997). These studies indicate the possibility of failure by delamination at the extremities of the reinforcement and the necessity of evaluating the long-term behavior. Structural elements with bonded and post-tensioned tendons exhibit greater strength and rigidity than elements in which the reinforcements are bonded, but not post-tensioned (McConnel et al. 2014).

This article presents a system that automatically produces a post-tensioning force proportional to the service loads to which the structure is subjected. The advantage of the presented system, and its main difference from other existing systems, is that the post-tensioning force is generated via the gravitational loads that act on the structure. Therefore, the system does not require any additional machinery or labor to introduce the post-tensioning force; it is automatically adjusted at every moment as the loads increase or decrease. Besides, the self-tensioning helps to limit the incidence of the prestress losses associated with traditional pre-tensioning systems (Davies and Fragiacomo 2011). When combined with a conventional pre-tensioning system, the proposed system can be of great utility when applied to the design of long-span wooden structural systems. It is possible to achieve structures that remain almost horizontal without significant deflections under service loads.

2. Description of the system

Over the course of the 20th century, the great advances of wood technologies have allowed the development of long-span structural elements capable to compete in terms of strength with other structural materials, such as steel or concrete. One of the limitations of these systems arises when it comes to consider the lower elastic modulus of wood and its derivative materials in comparison with other materials that are typically used in buildings. In the practice, this limitation means both limited bending stiffness and an additional difficulty when making rigid joints that can work to reduce bending in horizontal structural elements and overall deformations in frameworks. Traditionally, this limitation has been avoided either by increasing the height of the structural element in order to increase their bending stiffness or by manufacturing them with beam precambers which help to limit the net final deflections, known as appearance deformations.

This system of geometric beam precambers, created during the fabrication process, has several limitations. Firstly, it can be difficult to manufacture panels and mixed cross-sections with a precamber. Secondly, the value of the precamber should not exceed the maximum deflection allowed by the regulations for wooden structures.

These can vary between 1/150 and 1/500 of the span of the beam (L), depending on the scenario. The use of the precamber does not limit the maximum deflections that are associated with the assessment of integrity of the constructive elements. It takes into account the effects of both permanent and variable actions that occur after the execution of the concerned element.

The performance is slightly better when using an eccentric pre-tensioning system to generate a negative moment at the supports instead of the abovementioned manufactured geometric precamber. In this case, besides obtaining an instantaneous pre-camber ($\omega_{c,inst}$) that compensates the deformations due to the gravitational loads, it also limits the rotations at the supports and the overall deformations of the structure. Additionally, a favorable effect is expected due to creep deformations ($\omega_{c,creep}$) associated with the permanent character of the pre-tensioning force, which increase the precamber effect over time (Fig. 1) since the losses of prestress are expected to be neglected in elements loaded in parallel to the grain (Davies and Fragiacomo 2011). This favorable effect has not yet been systematically studied in timber, but is well known in prestressed concrete elements. The final deformations of the element after bearing loads are lower when the precamber is produced by pre-stressing rather than when using an initial geometric precamber of equal value. However, both cases suffer from similar problems due to the total deformations (from the precamber deflection to the net final deflection).

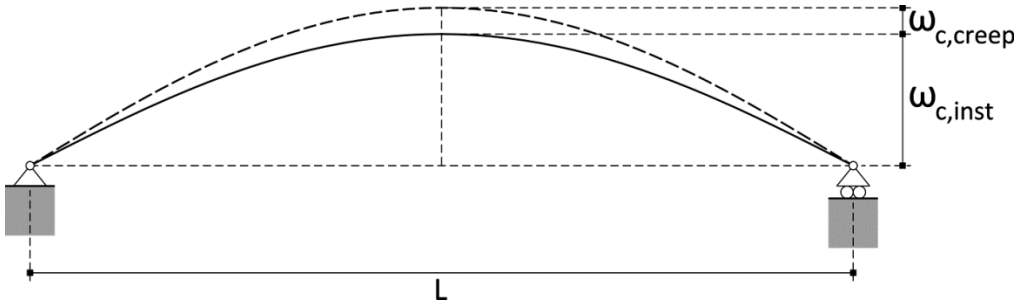

Fig. 1. Instantaneous and creep deflection generated by eccentric pre-tensioning.

This article presents an automatic self-tensioning system that is generated from the gravitational loads that act on horizontal structural elements (beams and/or frames). Placing the self-tensioning tendon eccentrically respect to the center of mass of the cross-section provides the same advantages of beam precambers as the ones obtained by pre-tensioning. Additionally, it has the favorable effect that the self-tensioning intensity varies depending on the service loads bear by the structural elements. The system uses a device at the supports of the structural elements. It is capable to convert the vertical reaction forces at the support into a tensile force in relation to the longitudinal axis of the horizontal structural element (Fig. 2).

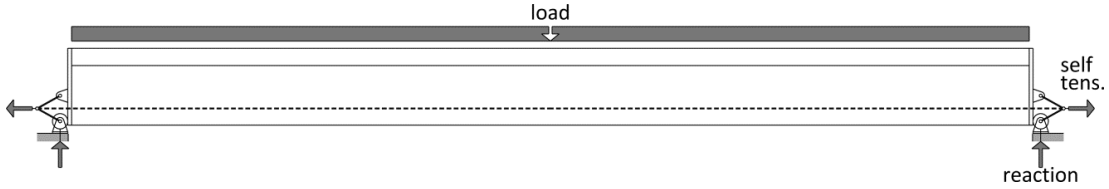

Fig. 2. Self-tensioning devices at the supports of the structural element.

This device can have different forms and be mechanical or hydraulic. As an example, an easily implementable mechanical device is proposed that consists of two connecting rods placed at each of the beam supports. The device is schematically shown in Fig. 3.

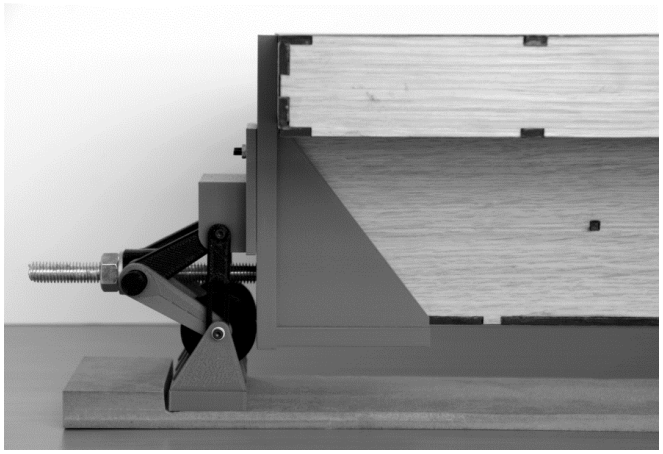

Fig. 3. 3D-Prototype of the mechanical device.

The system of connecting rods is maintained in equilibrium through an axial force in the post-tensioning bar (N), as shown in Fig. 4. In this way, the structural element transmits a force (F) to the device, thus giving rise to the corresponding reaction in the support (R) and to a self-tensioning force (N). This force equilibrium comes with a deformation of the device and a reduction in the angle α formed by the connecting rods. This means a vertical displacement at the support ($s=2\cdot\Delta z$), here and after referred as a support seat, and a subsequent lengthening of the post-tensioning bar ($\delta=\Delta L/2$).

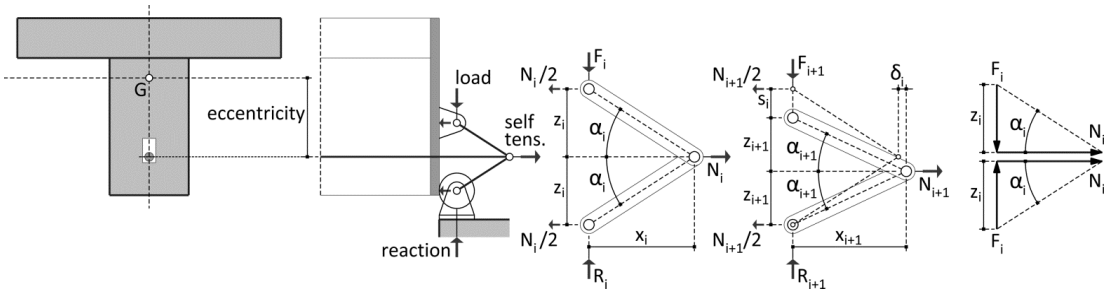

Fig. 4. Operational scheme for the self-tensioning device that is located at the supports.

The lengthening is translated into a post-tensioning axial force (N). When the loads acting on the beam decrease, the self-tensioning tendon regains its position and adjusts the intensity of the tensioning to the value of the service loads at each moment. In the solution proposed in this study, the self-tensioning system is combined with an initial conventional pre-tensioning to obtain the optimum performance of the structural element.

The eccentric placement of the tensioning tendons with respect to the center of mass of the cross-section generates a negative moment at the beam support. This moment provides a double benefit in terms of the deformation for simply supported

components of long spans. Firstly, the beam precamber counteracts the deformation due to the gravitational loads that act on the structural element. In addition, the negative moment at the support has the effect of a rigid joint and limits its rotation, which is difficult to achieve using conventional joints with fasteners in wooden structures due to the so-called problem of joint slippage.

Because the moment increases with the eccentricity of the tensioning tendons with respect to the center of mass of the cross-section (*G*), the efficiency of the proposed system increases in cases of asymmetric cross-sections, such as the one shown in Fig. 5, although it is valid for any type of cross-section. The proposed section can be used to design the entire horizontal framework (web member and flange) with the repetition of an only one module.

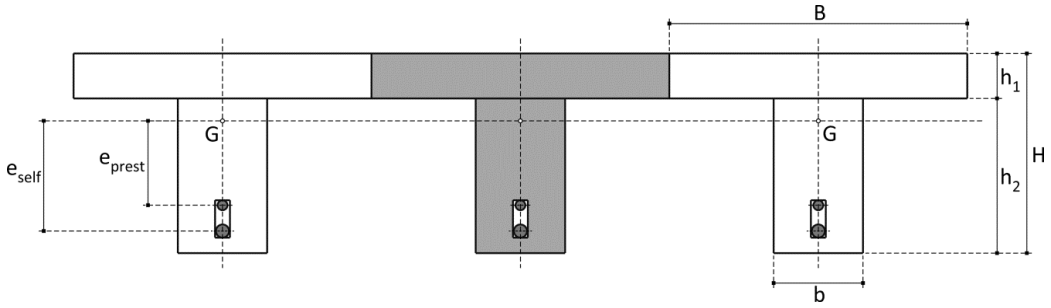

Fig. 5. Proposed piece with an asymmetric cross-section with respect to the center of mass.

As schematically shown in Fig. 4, the relationship between the reaction at the support (R) and the self-tensioning axial force (*N*) can be calculated based on the geometric relationship between the horizontal and vertical projections of the connecting rods (*x, z*) as a function of the angle (α) that they form at each specific loading state (*i*):

$$2 \cdot R_i / N_i = \sin\alpha_i / \cos\alpha_i = \tan\alpha_i \quad (1)$$

For a given loading state (*i*), the self-tensioning force (*Ni*) can be expressed as:

$$N_i = 2 \cdot R_i / \tan\alpha_i \quad (2)$$

Alternatively, the load multiplying factor ($\aleph_i$) can be expressed as:

$$\aleph_i = N_i / R_i = 2 / \tan\alpha_i \quad (3)$$

This multiplying factor ($\aleph_i$) helps to determine the value of the self-tensioning force (N_i) that is obtained for a given loading scenario (*i*). Eq. (3) and the geometric proportions that are shown in Fig. 4 demonstrate that the multiplier effect ($\aleph_i$) increases as the angle between the connecting rods (α_i) decreases.

Furthermore, the multiplier effect is not linear; as shown in Fig. 4, the self-tensioning force (N_i) calculated from Eq. (2) implies an increase in the tendon length (δi), which changes the geometry of the device, reduces the angle between the connecting rods (α_i) and, therefore, increases the multiplier effect at a later state of loading ($\aleph_{i+1}$). This increase in length (δ_i) and in the geometric change in the proportions of the system is given by:

$$\delta_i = \Delta L_i / 2 = N_i \cdot L / 2 \cdot E \cdot \Omega \quad (4)$$

where L is the tendon length, E is the longitudinal elastic modulus of the tendon, and Ω is the tendon cross-section.

In the case of rods, axial shortening produced by compression is neglected because it represents a much lower value than the tendon strain and it results in a considerably simplified analysis. The same can be considered with respect to the longitudinal shortening of the wooden piece, providing in any case a favorable effect on the system by leading to a smaller angle between the rods.

The negative moment that is produced in the support via the self-tensioning effect ($M_{self,i}$) at each moment of loading (i) will be:

$$M_{self,i} = N_i \cdot e_{self} = R_i \cdot \mathfrak{X}_i \cdot e_{self} \quad (5)$$

where *eself* is the eccentricity of the self-tensioning tendon with respect to the center of mass of the cross-section (Fig. 5).

3. Performance of the system

To illustrate the operation of the system, the behavior of a structural element with a T-shaped cross-section is analyzed (Fig. 5), which allows the use of one component to solve the supporting elements and the floor slab. A span of L=12 m is assumed to extend between the supports. For the total height of the section (H), a proportion of H=0.03L=360 mm is chosen, which is much less than the normal dimensions involved in this type of component to highlight the advantages of the system. A flange piece with a thickness h_1=90 mm is utilized, helping to meet the structural requirements of the floor slab and yielding a web element height of h_2=270 mm. The pieces of the flange have a width of B=600 mm, which easily adjusts to the moduli used to make this type of piece. The webs, which have a total width of b=180 mm, are manufactured as two 90-mm-wide pieces in which an intermediate groove is made to accommodate the pre-tensioning and self-tensioning tendons. The dimensions of the groove are designed to allow the tendons to be properly located, and besides, giving an additional clearance that allows the self-tensioning tendon to move as the support suffers the semi-seat. As discussed previously, the effectiveness of the self-tensioning system varies in accordance with the x and z-axis proportions of the rods (Fig. 4). This preliminary analysis used an initial proportion of x_o=100 mm and z_o=50 mm, which implies an initial angle between the rods in the device of α_o=26.6º. The effectiveness of these proportions is evaluated below. The flange is made of cross-laminated timber (CLT) from spruce timber with a strength class not below C18. The CLT-board used consists of three 30mm-thickness layers, being the most external ones parallel to the longitudinal axis of the floor element. The CLT-board has an average longitudinal elastic modulus of Emean=12,500 MPa (ETA 2014). The web is made with homogeneous glued laminated timber with a GL28h strength class and E_{mean}=12,600 MPa (CEN 2013). A homogenized cross-section is used for the analysis and to calculate the eccentricities of the tendons. These tendons are placed on the lower part of the section with only the amount of covering necessary to meet the required fire resistance, resulting in the maximum eccentricity values for the tensioning axial forces (e_{prest} and e_{self}).

Consistent with the proposed geometry, the initial multiplier effect ($\mathfrak{X}_0$) is equal to 4.0, which implies that the initial post-tensioning value is 4.0 times the reaction at each of the supports and that it increases as the load on the beam increases. To take this effect into account, an iterative incremental analysis was conducted at successive stages of loading. Thus, the geometric variation in the device at one stage (i) is considered in the next stage (i+1).

An initial pre-tensioning precamber value of $L/500$=24 mm is considered. This value implies that for an eccentricity of the pre-tensioning tendon of e_{prest}=131 mm, a pre-tensioning axial force of approximately 150.0 kN is introduced. A steel component (E=210,000 MPa) with a cross-section of Ω=700 mm2 is used as the self-tensioning tendon. As deduced from Eq. (4), the area of the self-tensioning tendon also influences the system's behavior. The performance of tendons with other cross-sections is analized in subsequent sections of the paper. The shape of the tendon is irrelevant; in practice, the self-tensioning element can take the form of one or several round shapes, solid squares, threaded rods, or plates. This pre-tensioned and self-tensioned solutions are compared with a floor section, called untensioned, that has the same T-shape with the same web and flange dimensions but in which neither tendons nor the groove to contain them are added.

To estimate the actions to which the structural element will be subjected to, an imposed load of Qk=3.0 kN/m2 is adopted, which is valid for administrative and public structures with furniture (CEN 2002), given that these large free span solutions are generally associated with public-use buildings. A value of Gk=2.0 kN/m2 is used for the permanent loads, which includes both the self-weight of the solution (self-weight ≈ 1.0 kN/m2) and the finishing materials.

For these initial conditions, the behavior of the multiplier system is analyzed in successive loading stages, as shown in Fig. 4, and explained in the previous paragraphs. Figs. 6 and 7 compare the deflections observed in an untensioned T-shaped solution and a T-shaped solution with an initial pre-tensioning and a variable self-tensioning using the proportions discussed previously, respectively.

The instantaneous deformations that correspond to the following loading stages were considered:

- H0: Load 0, initial position.
- H1: Permanent load, Gk=2.0 kN/m2.
- H2: Quasi-permanent load, Gk+ψ2·Qk=2.9 kN/m2.
- H3: Total load, Gk+Qk=5.0 kN/m2.

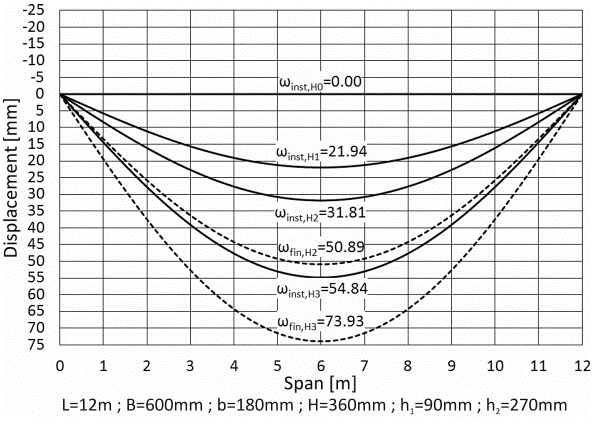

Fig. 6. Bending deformations at different loading stages (from H0 to H3) for an untensioned T-shaped element.

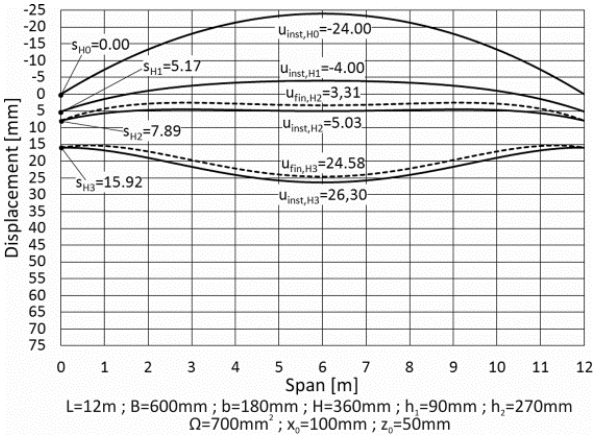

Fig. 7. Bending deformations at different loading stages (from H0 to H3) for a T-shaped element with pre-tensioning and self-tensioning.

Based on the estimated actions, a factor for the quasi-permanent loads of ψ_2=0.3 is used. Fig. 6 shows the values of the deflection (ω) of the untensioned section, and Fig. 7 shows the values of the displacements at the supports (s) and the midpoint of the beam (u) for the prestressed and self-tensioned section. The deflection (ω) for each hypothesis can be calculated as the difference between the displacement at the midpoint of the beam (u) and the displacement at the supports (s). In the case of the untensioned section, the deflection (ω) coincides with the displacement at the midpoint (u) since there are no seats at the supports.

The instantaneous deformation of the untensioned beam (Fig. 6) for the quasi-permanent loading scenario ($\omega_{inst,H2}$) is 31.81 mm, which implies a relative deflection of L/377. In the case of the pre-tensioned beam with the self-tensioning system, the displacement at the midpoint decreases to 5.03 mm. The self-tensioning system involves a seat of the support of 7.89 mm in this case. This movement implies a deflection of the beam (ω_{H2}) that is equal to the difference between the two values (i.e., 2.86 mm) and which is negative in this case. This deformation implies a relative deflection of L/4196, which indicates that the beam is almost horizontal in the quasi-permanent load scenario (H2).

The dashed lines represent the total deformations (ω_{fin}), which include the instantaneous and creep deformations from the quasi-permanent fraction of the load for the two preceding stages (H2 and H3).

The final deformation is calculated for each scenario as:

$$\omega_{fin} = \omega_{inst} + \omega_{creep} = \omega_{inst} + \Psi_2 \cdot \omega_{inst} \cdot k_{def} \quad (6)$$

A deformation factor of k_{def}=0.6 is used, which corresponds to service class 1. The comparison of the final deformations demonstrates the additional benefit of the creep deformation that is caused by the use of the tensioning tendons, which is schematically illustrated in Fig. 1. In this case, the final deflection of the untensioned beam for the same loading scenario ($\omega f_{in,H2}$) is 50.89 mm (L/236), and that for the self-tensioned beam is 7.89-3.31=4.58 mm (L/2620).

The introduction of the tensioning system also increases the strength because the maximum tensile stresses in the section are reduced. This reduction limits the possibility of brittle failure in the structural element and increases the overall bending strength of the floor, representing the most unfavorable stress for the design.

Both solutions have been verified under the ultimate limit states according to the Eurocode 5 (CEN 2013) criteria, yielding that bending and flexo-compression are the most unfavorable situations for the untensioned beam and for the self-tensioned beam, respectively. The interface web-flange is a critical point that could be solved by gluing, but its performance should be deeply studied in further experimental analysis. For the cases that concern us, the maximum stresses for a bending failure occur in the untensioned beam at a uniformly distributed load of 13.10 kN/m^2, while the self-tensioned section is able to support a load of 21.80 kN/m^2 before failing under flexo-compression, which implies a 66% increase in strength. However, the deformation criterion is much more restrictive.

The functioning of the self-tensioning system with respect to the applied loads for the same case study is illustrated in Figs. 8 and 9. Fig. 8 shows the variation of the multiplier effect as the load on the beam increases and the subsequent seat at the supports. The multiplier effect varies non-linearly based on the initial value $\aleph_0$=4.0,

which coincides with the initial geometry of the support of the device. For the maximum load of 5 kN/m2 (H3), the multiplier effect ( ) reaches a value of 4.92. The functioning of the system implies a seat at the support (s) and this value also increases nonlinearly as the load on the beam increases. Fig. 8 shows that both and *s* asymptotically approach infinity as the angle between the connecting rods (α) approaches zero. This position corresponds to the geometric nonlinearity of the system that would cause the collapse of the support; thus, it is necessary to establish a limit before this position is reached. For this case, the limit is taken to be equal to the dimension z0 minus 2 mm, which leads to a maximum possible seat of 96 mm. This high limit is excessive from the construction point of view, but it was adopted to illustrate the potential of the system. In the actual practice, it would be advisable to use a more restrictive limit to prevent failure since the performance under service loads does not change (Figs. 8 and 9). Once the multiplier device reaches this limit, it begins to behave as a conventional fixed support and maintains the self-tensioning that corresponds to the point of blockage. This behavior is shown in Fig. 9, which shows the instantaneous deformations for the untensioned section (linear with respect to the applied load) and for the beam with the self-tensioning system. For the beam with the self-tensioning system, the maximum displacement at the midpoint of the beam (*u*) and the relative deformation between the supports and the midpoint ($\omega=u-s$) are shown. In both graphs, the values that correspond to a load of 5 kN/m² (H3) are indicated to illustrate the correspondence with the deformations shown in Figs. 6 and 7. While the deflection in the untensioned beam reaches 54.84 mm, in the case of the beam with self-tensioning, the difference between the displacement at the midpoint of the span (u=26.30 mm) and the seat at the supports (s=15.92 mm) leads to a deflection of ω=10.38 mm (Figs. 6 and 7). This deformation implies a final deflection in the self-tensioned beam of less than 19% of that of the untensioned beam.

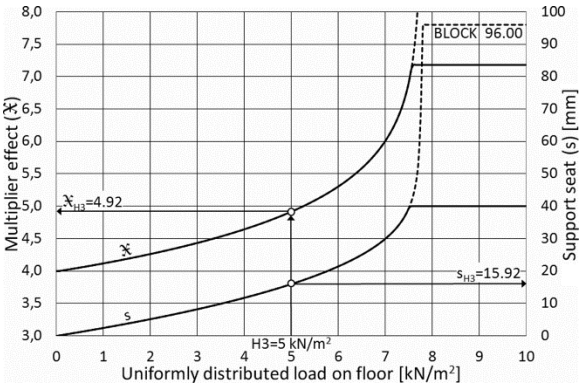

Fig. 8. Multiplier effect ( ) and support seats (s) for the self-tensioned beam as a function of the change in load.

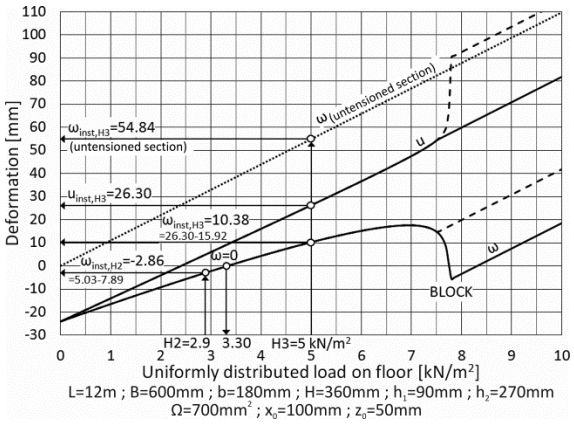

Fig. 9. Displacement of the midpoint (u) and deflection (ω) for the self-tensioned beam as a function of the change in load.

Fig. 9 allows the value of the creep deformation to be determined in accordance with Eq. (6). In the case of our concern, the deflection (ω) that corresponds to the quasi-permanent fraction of the load H2 (q_k=2.9 kN/m2) would be -2.86 mm (the negative sign indicates the upward direction). By applying Eq. (6) to the case of the total load, $\omega_{fin}=\omega_{inst}+k_{def}.\omega_{inst}(\psi_2.q_k)$=10.38+0.6·(-2.86), we obtain a final deformation of 8.66 mm for the total load, which is 11.7% of the 73.93 mm that corresponds to the

untensioned beam for the same scenario, and a relative deflection of $L/1386$. Due to the nonlinearity of the system, the determination of the creep deformation from the quasi-permanent fraction of the loads (H2) implies the analysis of the instantaneous deformation that corresponds to this fraction of the load instead of applying the factor ψ2 to the instantaneous deformation that corresponds to hypothesis H3.

Using these values as an example, Fig. 9 highlights the reduction in deflection (ω) of the self-tensioned beam with respect to the untensioned beam and how it improves the performance of the self-tensioning with respect to the untensioned beam as the load on the beam increases. Inversely, the figure can also be used to obtain the value of the load for which the deflection in the structural element is zero (ω=0), which in this case is for a uniformly distributed load of approximately 3.3 kN/m2.

4. Performance in different configurations

Assuming that the effectiveness of the self-tensioning system changes as a function of the initial geometry and the characteristics of the self-tensioning tendon, it is worth to study other solutions and to evaluate the ultimate performance of the system.

At first, the changes in the initial angle of the tensioning device (α_o) are analyzed based on a fixed dimension x_o=100. The remaining parameters of the beam are kept constant: L=12 m, B=600 mm, b=180 mm, h_1=90 mm, h_2=270 mm, and Ω=700 mm2. Fig. 10 shows the change in the multiplier effect ( ) for devices in which different angles are used between the pieces that constitute the connecting rods (α_0=20º, 25º, 30º, and 35º) and the corresponding seat at the supports (s). Fig. 11 shows the deformations of the untensioned beam for different values of the load, displacement (u) and relative deformation (ω) of the self-tensioned beam for different angles as similarly shown in Figs. 8 and 9. In all cases, the block point of the system is kept equal to z0-2 mm.

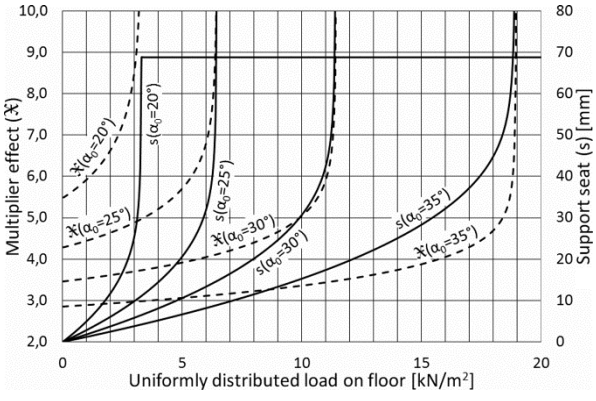

Fig. 10. Multiplier effect ( ) and seat of the support (s) for the self-tensioned beam as a function of the change in load for different initial angles between the connecting rods (α_0).

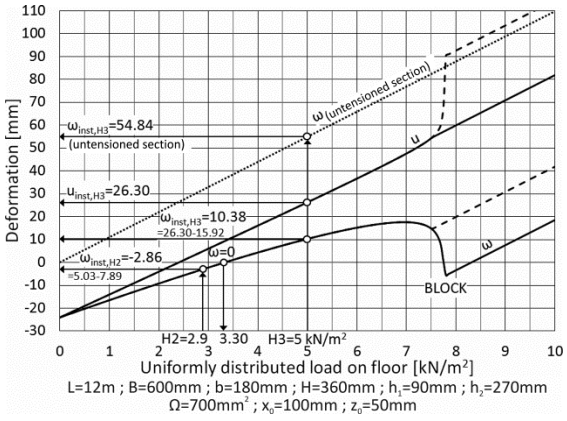

Fig. 11. Displacement of the midpoint (u) and deflection (ω) for the self-tensioned beam as a function of the change in load for different initial angles between the connecting rods (α_0).

The change in the initial angle (α_o) between the connecting rods that form the multiplier device has a significant impact on the effect of the device, which can be deduced from Eq. (3) and is shown in Figs. 10 and 11. A smaller initial angle implies not only a greater multiplier effect of the initial load ( ) but also a limitation in the

range of loads in which the device has an effect (Fig. 10). Thus, for an initial angle of α_o=20º, the initial multiplier effect is $\mathfrak{x}_0$=5.5. It increases rapidly at small loads, but the device reaches its limit at a smaller load (3.35 kN/m2). The greater multiplier effect implies that for a smaller initial angle, smaller deflections are obtained in the structural component for identical loads (Fig. 11). These reduced deflections occurred because both pre-tensioning and self-tensioning moments modify the bending behavior, making the negative moments at the support to overcome the moments in the center of the beam. This is illustrated in Fig. 12, which shows the characteristic values of the bending moments that correspond to a load of q_k=5.0 kN/m2 (H3).

On the other side, a small initial angle implies faster and greater seats at the supports. It means that the total displacement at the midpoint of the beam (u) is similar for all different angles, whenever the multiplier device does not reach its limit.

Fig. 13 shows the initial deformations (ω_{H0}, u_{H0}) and those for the total loading (ω_{H3}, u_{H3}) of the untensioned beam and of the self-tensioned beams with initial angles between the rods of α0=25º, 30º, and 35º. Figs. 11 and 13 show that the instantaneous deformation in the untensioned section is 54.84 mm (L/219) for the total load scenario. The deflections (ω) for self-tensioned sections with α0=25º, 30º, and 35º are 27.62-20.64=6.98 mm (L/1720), 25.09-10.64=15.05 mm (L/797), and 24.73-6.66=18.07 mm (L/664), respectively. However, the overall displacements (u) are very similar to the three self-tensioned solutions (between 27.62 (L/435) and 24.73 mm (L/485)) because, as explained above, a larger multiplier effect implies smaller deflections in the structural element but greater seats at the supports.

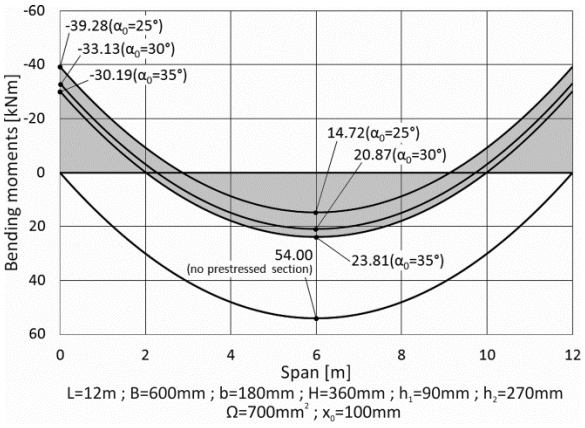

Fig. 12. Characteristic bending moments for a surface load of 5 kN/m2 for different initial angles between the connecting rods (α_0).

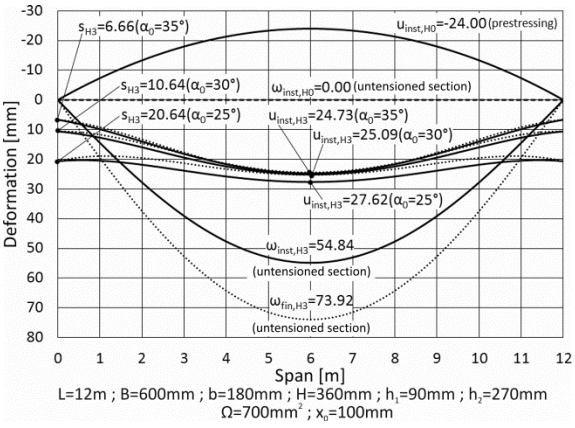

Fig. 13. Initial deformation (H0) and instantaneous (solid lines) and creep (dashed lines) deformations for the hypothesis of total loading (H3) for different initial angles between the connecting rods (α_0).

Fig. 14 shows that in addition to the decrease in the relative deformation, almost no creep deformation occurs with the self-tensioned system. This finding can be explained by the data presented in Fig. 11, which shows that the relative instantaneous deformations (ω_{inst}) for self-tensioning systems with α_o=25º, 30º, and 35º for the quasi-permanent loading scenario (H2) are very close to zero, which leads to almost no creep deformation in the total loading scenario (H3).

Specifically, the deflections for the hypothesis of quasi-permanent loads, q_k=2.9 kN/m², are -3.96, -1.13, and +0.63 mm for α_o=25º, 30º and 35º respectively. It implies creep deformations of -2.37 mm, -0.68 mm, and 0.38 mm as seen in Fig. 14;

nearly zero. Since only the quasi-permanent loads result in creep deformations, those nearly zero creep deformations are the same for all the service load scenarios. This is the situation between the quasi-permanent loading and the total loading hypotheses (between H2 and H3).

The improvement provided by the system also works in structural elements of larger spans. The deformations for an element with a span of 15 m are analyzed. The same geometric parameters that were proposed in the previous solution are considered. The proportion H=0.03L leads to a total height of H=450 mm and a web height of h_1=360 mm. To maintain a similar range of stresses in the post-tensioning element, the cross-section of the tendon is increased to Ω=900 mm2.

Fig. 15 shows the deformation values for the four initial angles (α_0=20º, 25º, 30º, and 35º) as a function of the surface load that acts on the element, and Fig. 16 shows the instantaneous and creep deformations for the total loading scenario (H3). The device with an angle α_0=20º would be once again insufficient for this range of loads and spans because the multiplier effect is exhausted for uniformly distributed loadings of less than 3.0 kN/m2, which leads to extensive seat at the support (s) for the total load. For α_0=25º, the multiplier device approaches the horizontal position for a load of 5.0 kN/m2. This case coincides with a nearly zero relative deflection of 2.01 mm (L/7463) but entails a significant seat of the support of 33.22 mm. The devices with angles of α_0=30º and 35º exhibit instantaneous deflections for total loadings of 17.43 mm and 22.57 mm (L/861 and L/665, respectively), which are nearly the same as the total deformation (including the creep). Fig. 15 shows that the instantaneous midpoint displacements for quasi-permanent loads of 2.9 kN/m2 are -5.54 mm, -1.51 mm, and +0.87 mm for angles of α_0=25º, 30º, and 35º, respectively. These results imply instantaneous relative deflections between L/2707 and L/17241 for the quasi-permanent loading scenario (H2), which indicates near horizontality under the service conditions.

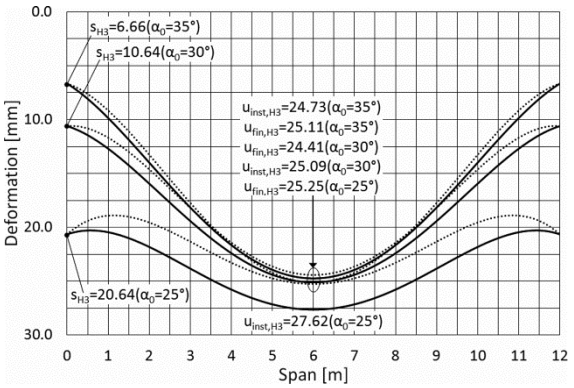

Fig. 14. Detailed view of Figure 13 showing the instantaneous (solid lines) and creep (dashed lines) deformations for elements with α0=25, 30 and 35º in a total loading scenario (H3).

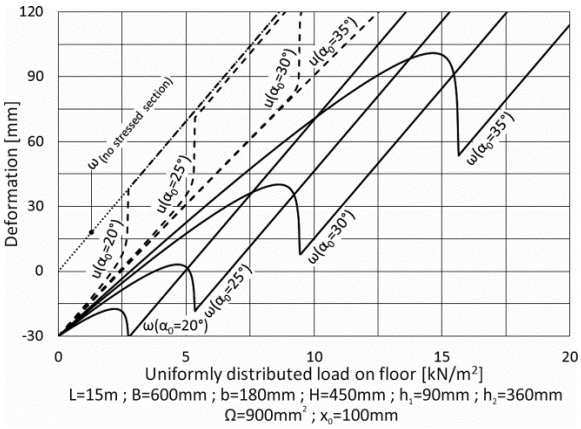

Fig. 15. Displacement of the midpoint (u) and deflection (ω) for the self-tensioned beam as a function of the change in load for different initial angles between the connecting rods (α_0).

Eqs. (1) and (4) show that the axial stiffness of the self-tensioning tendon also has a significant influence on the effectiveness of the multiplier device. For the initial case, a cross-sectional area of Ω=700 mm2 was used, which approximately corresponds to a solid round section that is 30 mm in diameter, although the tendon could respond

to any cross-sectional shape. For example, a multiplier effect of 4.92 for a total surface load of 5 kN/m2 (Fig. 8) would imply an axial force in the component of N=88.6 kN. Therefore, the tendon would be working in a reduced range of stresses (126.5 MPa) in terms of characteristic values.

However, the tendons must remain in the elastic regime to adapt to the behavior that is described in Eq. (4) and to ensure the possibility of destressing in the case of the unloading of the component.

To analyze the impact of the cross-section of the self-tensioning tendon (Ω), the initial device dimensions of x_0=100 and z_0=50 are kept constant, which make α_0=26.6º and χ_0=4.0. The initial proportions of the structural component with a T-shaped cross-section are maintained: L=12 m, B=600 mm, b=180 mm, h_1=90 mm, and h_2=270 mm. Tensioning components of any shape (e.g., round, square, plate) could be used in practice as long as their areas are equivalent to solid round sections with diameters of Ø=16 mm, 20 mm, 24 mm, 30 mm, and 36 mm.

A smaller diameter (Ø), or equivalently a smaller cross-section Ω, implies a faster increase in the multiplier effect (χ) but also a more extensive seat at the supports (s) (Fig. 17). For a load of 2.0 kN/m2, the multiplier effect varies between 5.77 for a tendon of Ø=16 mm and 4.17 for a tendon of Ø=36 mm, while the seat of the supports varies between 28.29 mm for the smaller-diameter bar and 3.45 mm for the larger-diameter bar. As shown in Fig. 18, these results indicate that bars with smaller cross-sections have lower deflections (ω) but greater displacements at the midpoint of the structural element (u).

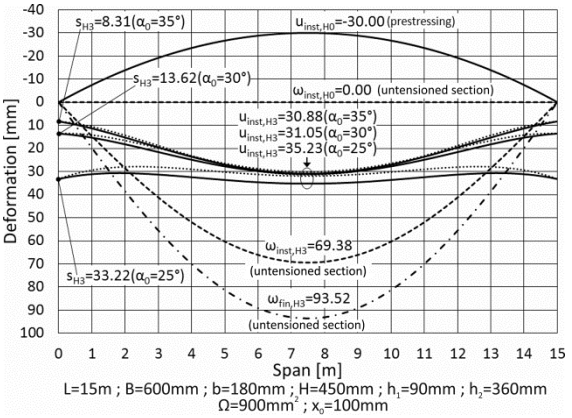

Fig. 16. Initial deformation (H0) and instantaneous (solid lines) and creep deformations (dashed lines) for the total loading (H3) for different initial angles between the connecting rods (α_0).

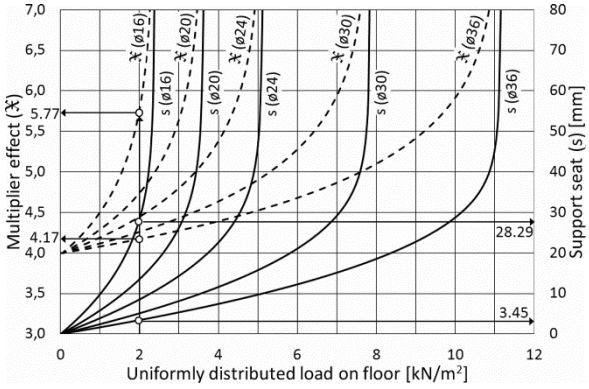

Fig. 17. Multiplier effect ( ) and seat of the support (s) for different diameters of the self-tensioning tendon (Ø).

Fig. 19 shows the instantaneous deformations for a load of 2.9 kN/m², which corresponds to the quasi-permanent fraction of the load (H2). The deflection of the self-tensioned sections varies between 5.74 mm (L/2090) for Ω=Ø20 and 2.35 mm (L/5106) for Ω=Ø36 compared to the deflection of 31.81 mm (L3/77) that corresponds to the untensioned section. However, the relative deformations increase more slowly as the cross-section of the self-tensioning tendon decreases (Fig. 18). As a result, the selection of the tendon's cross-section could be easily adapted to the range of service loads of the structural component.

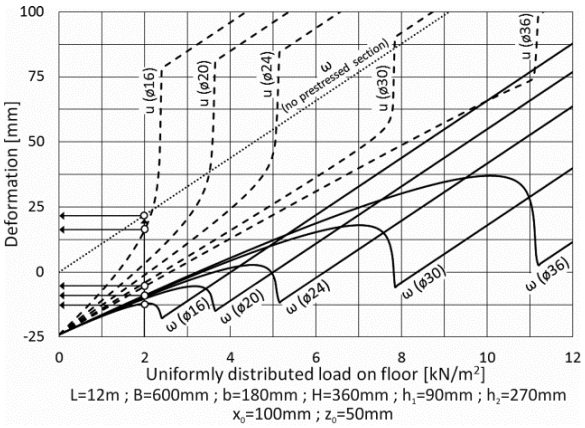

Fig. 18. Displacement of the midpoint (u) and deflection (ω) for different diameters of the self-tensioning tendon ($Ø$).

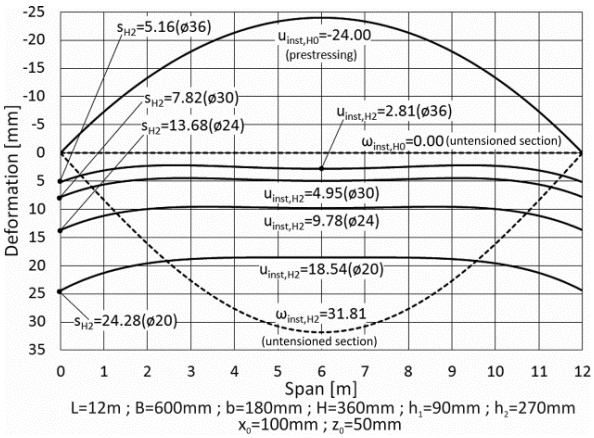

Fig. 19. Instantaneous deformation for a load of 2.9 kN/m² (H2) for different diameters of the self-tensioning tendon ($Ø$).

Conclusions

A self-tensioning system that converts the gravitational loads that act on horizontal structural elements into a post-tensioning force was developed. This study proposes one possible mechanical solution for the construction of this self-tensioning system that is based on articulated rods.

The efficiency of the self-tensioning system that is presented in this study depends on the geometric proportions of its components and on the axial stiffness of the tendon involved.

By using a self-tensioning tendon that is eccentric to the cross-section and combining it with conventional pretensioning, it is possible to design structural long-span elements with relative deflections throughout their service life below 1/1000 of the span and heights of 0.03 of the span.

An extensive experimental analysis would verify the performance of the self-tensioning system proposed in this paper in the future.

Acknowledgements

This study is part of a research project entitled “High-performance prefabricated systems of pretensioned wood laminate with non-bonded tendons”, financed by the Ministry of Economy and Competitiveness of the Kingdom of Spain and the European Fund for Regional Development.

Notation list

The following symbols are used in this paper:
B = width of the flange of the T-shaped floor element;
b = width of the web member of the T-shaped floor element;
E = modulus of elasticity;
e_{prest} = eccentricity of the pre-tensioning tendon with respect to the center of mass of the cross-section;
e_{self} = eccentricity of the self-tensioning tendon with respect to the center of mass of the cross-section;
F = load on the support;
G = center of mass of the cross-section;

H = total height of the T-shaped floor element, H=h1+h2;
H0-H3 = loading stages;
h1= height of the flange of the T-shaped floor element;
h2= height of the web member of the T-shaped floor element;
L = span of the structural element;
M_{self} = moment produced on the support via the self-tensioning effect;
N = self-tensioning force;
R = reaction at the support;
s = downward movement or seat at the support;
u = deformation, displacement of the midpoint of the structural element;
x = length of the horizontal projection of the connecting rods in the self-tensioning device;
z = length of the vertical projection of the connecting rods in the self-tensioning device;
α = angle between the connecting rods in the self-tensioning device;
δ = increase in length of the self-tensioning tendon;
ψ2 = factor for the quasi-permanent value of variable loads;
Ω = cross-sectional area of the self-tensioning tendon;
ω = deflection or relative deformation, displacement of the midpoint of the element with respect to a straight line between the supports;
$\omega_{c,creep}$ = creep deformation from a precamber obtained by prestressing;
$\omega_{c,inst}$ = instantaneous precamber obtained by prestressing;
ω_{creep} = creep deflection;
ω_{inst} = instantaneous deflection:
ϰ = multiplier effect;

References

Alhayek, H., Svecova, D. (2012). "Flexural stiffness and strength of GFRP-reinforced timber beams." Journal of Composites for Construction, 10.1061/(ASCE)CC.1943-5614.0000261, 245-252.

Borri, A., Corradi, M., Speranzini, E. (2013). "Reinforcement of wood with natural fibers." Composites Part B: Engineering, 53, 1-8.

Brunner, M., Schnüriger, M. (2004). "Timber beams strengthened with prestressed fibres: Delamination." Proc., 8th World Conf. on Timber Engineering.

Buchanan, A., Palermo, A., Carradine, D., Pampanin, S. (2011). "Post-tensioned timber frame buildings". Structural Engineer, 89 (17), 24-30.

CEN (European Committee for Standardization). (2002). "Eurocode 1: Actions on structures – Part 1-1: General actions – Densities, self-weight, imposed loads for buildings." EN 1991-1-1.

CEN (European Committee for Standardization). (2013). "Timber structures. Glued laminated timber and glued solid timber. Requirements." EN 14080.

D'Ambrisi, A., Focacci, F., Luciano, R. (2014). "Experimental investigation on flexural behavior of timber beams repaired with CFRP plates." Composite Structures, 108(1), 720-728.

Davies, M., Fragiacomo, M. (2011). "Long-term behavior of prestressed LVL members. I: Experimental tests." Journal of Structural Engineering, 10.1061/(ASCE)ST.1943-541X.0000405, 1553-1561.

De La Rosa García, P., Escamilla, A.C., Nieves González García, M. (2013). "Bending reinforcement of timber beams with composite carbon fiber and basalt fiber materials." Composites Part B: Engineering, 55, 528-536.

Dolan, C.W., Galloway, T.L., Tsunemori, A. (1997). "Prestressed glued-laminated timber beam - Pilot study." Journal of Composites for Construction, 1 (1), 10-16.

ETA (European Technical Assessment) (2014). "CLT – Cross Laminated Timber." ETA-14/0349.

Gesualdo, F.A.R., Lima, M.C.V. (2012). "An initial investigation of the inverted trussed beam formed by wooden rectangular cross section enlaced with wire rope". Structural Engineering and Mechanics, 44(2), 239-255.

Iqbal, A., Pampanin, S., Palermo, A., Buchanan, A.H. (2014). "Behaviour of post-tensioned timber columns under Bi-directional seismic loading." Bulletin of the New Zealand Society for Earthquake Engineering, 47(1), 41-53.

Kliger, R., Al-Emrani, M., Johansson, M., Crocetti, R. (2008). "Strengthening timber with CFRP or steel plates - Short and long-term performance." Proc., 10th World Conf. on Timber Engineering, T. Arima, ed., Vol.1, 414.421.

Long, M. (2010). "Richmond Olympic Oval." Acoustics today, 6(1), 8-11.

McConnell, E., McPolin, D., Taylor, S. (2014). "Post-tensioning of glulam timber with steel tendons". Construction and Building Materials, 73, 426-433.

Morris, H., Wang, M., Zhu, X. (2012). "Deformations and loads in an LVL building with 3-storey post-tensioned shear walls." Proc., 12th World Conference on Timber Engineering, Vol.3, 110-117.

Palermo, A., Pampanin, S., Carradine, D., Buchanan, A.H., Dal Lago, B., Dibenedetto, C., Giorgini, S., Ronca, P. (2010). "Enhanced performance of longitudinally post-tensioned long-span LVL beams." Proc., 11th World Conference on Timber Engineering, Vol.1, 449-459.

Smith, T., Ponzo, F.C., Di Cesare, A., Pampanin, S., Carradine, D., Buchanan, A.H., Nigro, D. (2014). "Post-tensioned glulam beam-column joints with advanced damping systems: Testing and numerical analysis." Journal of Earthquake Engineering, 18(1), 147-167

Triantafillou, T.C., Deskovic, N. (1992). "Prestressed FRP sheets as external reinforcement of wood members." Journal of structural engineering New York, N.Y., 118(5), 1270-1284

Van Beerschoten, W., Palermo, A., Carradine, D., Pampanin, S. (2012) "Design procedure for long-span post-tensioned timber frames under gravity loading". Proc., 12th World Conference on Timber Engineering, Vol.1, 354-361.

Wanninger, F., Frangi, A. (2014). "Experimental and analytical analysis of a post-tensioned timber connection under gravity loads." Engineering Structures, 70, 117–129.